Modeling the Structure and Composition of Nanoparticles by Extended X-Ray Absorption Fine-Structure Spectroscopy

Anatoly I. Frenkel, Aaron Yevick, Chana Cooper, and Relja Vasic

Department of Physics, Yeshiva University, New York, New York 10016;
email: anatoly.frenkel@yu.edu, aaronjmy@gmail.com, chanacoop@gmail.com, rvasic@bnl.gov

Annu. Rev. Anal. Chem. 2011. 4:23–39

First published online as a Review in Advance on February 22, 2011

The *Annual Review of Analytical Chemistry* is online at anchem.annualreviews.org

This article's doi:
10.1146/annurev-anchem-061010-113906

1936-1327/11/0719-0023$20.00

Keywords

coordination numbers, structure, shape, composition, disorder

Abstract

Many metal clusters in the 1-nm size range are catalytically active, and their enhanced reactivity is often attributed to their size, structure, morphology, and details of alloying. Synchrotron sources provide a wide range of opportunities for studying catalysis. Among them, extended X-ray absorption fine-structure (EXAFS) spectroscopy is the premier method for investigating structure and composition of nanocatalysts. In this review, we summarize common methods of EXAFS analysis for geometric and compositional characterization of nanoparticles. We discuss several aspects of the experiments and analyses that are critical for reliably modeling EXAFS data. The most important are sample homogeneity, the width of the size and compositional distribution functions, and accounting for multiple-scattering contributions to EXAFS. We focus on the contribution of structural disorder and structural/compositional heterogeneity to the accuracy of three-dimensional modeling.

1. INTRODUCTION

EXAFS: extended X-ray absorption fine-structure

STEM: scanning transmission electron microscopy

HAADF: high-angle annular dark field

The unique physical and chemical properties of nanometer-sized metal particles, in particular their enhanced catalytic activity, are an active subject of research. Pending the development of accurate imaging methods that can locate atoms in nanometer-sized catalysts, especially when studied in reaction conditions, researchers must resort to indirect structure-sensitive techniques. Accordingly, some relevant and intriguing questions are (*a*) whether nanoparticles can be characterized in terms of particular polyhedral shapes, and if so, what shapes exist in a given sample, and (*b*) whether these obtained shapes are unique. The solutions to these problems are both difficult and nonunique because the answers depend on many internal and external variables, such as temperature, gas atmosphere and pressure, ligands and adsorbates, support material, and alloying elements. These and other challenges, such as the insufficient spatial and temporal resolution of many experimental techniques, have also motivated the development of new approaches and instrumentation that are optimized for structural investigations of nanomaterials.

Soon after extended X-ray absorption fine-structure (EXAFS) spectroscopy was first introduced by Sayers et al. (1) as a structural technique, its potential for solving the structure of nanoparticles was recognized (2–5). EXAFS is one of the best tools with which to study both atomic and electronic structure of small ensembles, due in part to its local structure sensitivity and excellent spatial resolution. By measuring coordination numbers, bond lengths, and disorder up to the fifth coordination shell, the size and shapes (e.g., oblate, raft-like, or truncated polyhedral) of nanoparticles, as well as the surface morphology and disorder of 1–2-nm clusters, can be analyzed as a function of external conditions such as temperature, alloy composition, and substrate material.

Complementary information about site-specific structure and chemistry can also be obtained by scanning transmission electron microscopy (STEM), which has the unique capability of providing structural and spectral information simultaneously. Supported metal nanoclusters ranging from 1 to 100 atoms in size are ideal for examination by high-angle annular dark field (HAADF) imaging. Correlating the absolute image intensity to the scattering cross section has recently been advanced through STEM-based imaging methods (6, 7). This improvement makes it possible to directly count, with an accuracy of ± 2 atoms, the number of atoms in a supported nanocluster, thereby avoiding complexities arising from coherent diffraction. With state-of-the-art electron and X-ray probe methods, one can explore both substrate-nanoparticle interactions as a function of substrate and nanoparticle materials and the size, composition, and three-dimensional structure of the nanoparticles.

Given the progress in the development of the EXAFS and STEM techniques and data-analysis methods, as well as the availability of third-generation synchrotrons and aberration-corrected transmission electron microscopes, we may be tempted to conclude that the problem of solving nanoparticle structures is close to a solution. But is it? Have we overcome other obstacles, of which the lack of a well-defined methodology of nanoparticle-structure refinement and the lack of proof that the resulting model (or models) is unique are the most severe? Addressing these issues is the main purpose of this review.

In Section 2, we briefly overview EXAFS analysis methods. In Section 3, we survey recently developed techniques for obtaining the shape, size, and morphology of nanoparticles through EXAFS data modeling. Finally, in Section 4, we discuss factors that limit the precision of EXAFS analysis and propose algorithms for improving its accuracy.

2. EXTENDED X-RAY ABSORPTION FINE-STRUCTURE ANALYSIS

In the EXAFS technique, information about the electronic properties and structural environment of the X-ray absorbing atom and its surroundings is extracted from the X-ray absorption coefficient,

$\mu(E)$, measured within 1,000–1,500 eV of the X-ray absorption edge energy, that is, the excitation energy of the core-level electron. This energy range contains the X-ray absorption near-edge structure and EXAFS spectra. The oscillatory part of $\mu(E)$, also known as the EXAFS signal, or $\chi(k)$, is obtained by normalizing the $\mu(E)$ by the edge step and subtracting the smooth background function. These oscillations, which arise from the interference patterns of photoelectrons due to their scattering from neighboring atoms, contain quantitative information about the atomic environment in the proximity of the absorbing atom. The EXAFS signal contains the sum of all contributions, $\chi_i(k)$, from groups of neighbors at approximately equal distances from the absorbing atoms (i.e., within the ith shell), which are often written as (8)

$$\chi_i(k) = \frac{S_0^2 n_i}{k R_i^2} |f_i^{\text{eff}}(k)| \sin\left[2kR_i - \frac{4}{3}\sigma_i^{(3)}k^3 + \delta_i(k)\right] e^{-2\sigma_i^2 k^2} e^{-2R_i/\lambda_i(k)}, \quad (1)$$

where k is the photoelectron wave number; $f_i^{\text{eff}}(k)$ and $\delta_i(k)$ are the photoelectron scattering-path amplitude and phase, respectively; S_0^2 is the passive electron-reduction factor; n_i is the degeneracy of the scattering path; R_i is the effective half–path length (which equals the interatomic distance for single-scattering paths); σ_i^2 is the mean-square deviation in R_i; $\sigma_i^{(3)}$ is the third cumulant of the pair distribution function (9); and $\lambda_i(k)$ is the photoelectron mean free path. The mean-square deviation, σ^2, of the first-nearest-neighbor (1NN) distance can be represented to a good approximation as a superposition of static (σ_s^2) and dynamic (σ_d^2) terms:

$$\sigma^2 = \langle (r - \langle r \rangle)^2 \rangle = \sigma_s^2 + \sigma_d^2. \quad (2)$$

By obtaining the best-fit values, along with their uncertainties of n_i, R_i, σ_i^2, and $\sigma_i^{(3)}$, one can significantly reduce the number of possible models of cluster structure and their interaction with the environment (thermal effects, gas atmosphere effects, cluster-substrate and cluster-adsorbate interactions, etc.). However, EXAFS yields only ensemble-averaged information, and thus its application is most valuable for structural refinement of size-controlled nanoclusters. In this review, we specifically address the meaning of EXAFS results obtained for clusters whose size and compositional distributions are not symmetric or narrow.

The most dominant contribution to EXAFS signal is from backscattering of the photoelectron by neighboring atoms toward the absorbing atom (so-called single scattering). More complex scattering patterns involve reflections of the electron wave off of multiple atoms (10). This multiple-scattering approach is necessary to accurately calculate the absorption coefficient. For example, the contribution from multiple scattering by atoms along an atomic row, known as the shadowing or focusing effect, can dominate the backscattering. The amplitude-reduction factor, S_0^2, describes the intrinsic losses upon excitation that arise due to the many-body effects in the photoabsorption process.

The σ_i^2 term reduces the intensity of EXAFS oscillations at high k as a consequence of fluctuations in interatomic distances. It equals the standard deviation in the bond length and is caused by configurational (temperature-independent) disorder and dynamic vibrations. Although commonly used in EXAFS analysis as a measure of the bond-length disorder, this term is applicable only to systems with small to moderate disorder, for which the first few terms in the cumulant expansion of the pair distribution function adequately represent the unknown distribution (11). High-order cumulants in EXAFS analysis generally describe the asymmetry in the pair distribution function beyond the Gaussian approximation (9), but whether cumulants of order four and higher can be reliably extracted from data remains an unresolved issue (12). Neglecting the anharmonic term (Equation 1) yields a nonphysical decrease in the 1NN bond lengths at high temperatures and can be confused with the real negative thermal expansion that has recently been observed in nanoparticles (13, 14). To separate the temperature-independent σ_s^2 and temperature-dependent σ_d^2, one

may employ various phenomenological models, such as the correlated Einstein (15) and correlated Debye (16) models.

To extract these and additional structural parameters from experiments, the theoretical EXAFS equation (Equation 1) must be fit to the measured data. The number of adjustable parameters should not exceed the number of relevant independent data points in the analysis: $N_{idp} = 2\Delta k \Delta r/\pi$ (17). The analysis can be performed by a number of software packages that both perform nonlinear least-square fitting and report uncertainties in the results. Among the most popular programs based on ab initio calculations of X-ray absorption spectra are IFEFFIT (18), EXCURVE (19), and GNXAS (20).

A common strategy for analyzing mono- and multimetallic nanoparticles involves first obtaining the passive electron-reduction factor (S_0^2) from a fit to a bulk standard (e.g., a metal foil), then fixing it in the subsequent fits to the nanoparticle data to obtain coordination numbers. Multiple-scattering analysis allows for measurements of coordination numbers within the first five shells in the face-centered cubic (fcc) structure in monometallic (21) and bimetallic (22) nanoparticles. The latter analysis is performed by constraining the heterometallic bonds to have the same bond lengths and disorder parameters, as viewed from either metal-absorption edge (23). Furthermore, the following constraint on the coordination numbers of heterometallic bonds around elements A and B is used: $n_{AB} = n_{BA}(x_B/x_A)$, where x_A and x_B are the bulk concentrations of elements A and B, respectively (24).

3. SOLVING THE NANOPARTICLE STRUCTURE BY EXTENDED X-RAY ABSORPTION FINE-STRUCTURE ANALYSIS

In studies of the structure of nanoparticles, the coordination numbers n_i (Equation 1) are considered to be the most important structural parameters that can be obtained from EXAFS analysis. The coordination number of the ith shell (with radius R_i) around the absorbing atom in a monometallic cluster is defined as the average number of nearest neighbors within a given shell per absorber:

$$n_i = \frac{2N_i}{N}. \tag{3}$$

Here N_i is the total number of the nearest neighbors separated by R_i, and N is the total number of absorbing atoms in the cluster. In a heterometallic cluster, Equation 3 describes the coordination number $n_{AA(i)}$ of monometallic pairs:

$$n_{AA(i)} = \frac{2N_{AA(i)}}{N_A}. \tag{4}$$

The coordination number $n_{AB(i)}$ of the heterometallic pairs A and B is defined as

$$n_{AB(i)} = \frac{N_{AB(i)}}{N_A}, \tag{5}$$

where N_A is the total number of A atoms in the cluster. The numerator in Equation 4 contains a factor of two because each of the two atoms in the monometallic pairs can absorb X-ray photons, so such pairs should be counted twice.

Coordination numbers are obtained by EXAFS analysis model independently and are often employed for characterizing the clusters in terms of their structure and geometry. However, as described below, such interpretation should be done with extreme caution because the actual clusters in any given sample display a range of sizes and compositions. The ensemble averaging is done within the EXAFS experiment, and that averaging may not be representative of any given

cluster if the composition or size distributions are broad and/or if the clusters are disordered, as demonstrated below.

To establish a clear picture of the particle structure and shape, EXAFS analysis of coordination numbers must extend to higher-order shells (21, 22, 25) by including single- and multiple-scattering contributions from these shells to the EXAFS data. With this approach, coordination numbers can be obtained up to the fifth shell (21, 25), although with less accuracy than for the first shell.

Numerous methods have been developed to correlate the coordination numbers obtained from EXAFS with the size, structure, and shape of nanoparticles. In one such approach, the experimentally obtained sequence of coordination numbers measured by EXAFS analysis is compared with the same sequence calculated theoretically for a given cluster model. For cluster modeling, a number of methods employ closed-shell clusters based on regular polyhedra. These models utilize exact analytical relationships between the size (and hence the magic number of atoms and the polyhedral order) of the cluster and the coordination number of any given shell. Greegor & Lytle (26) developed analytical equations to obtain first-shell coordination numbers for various shapes, including spheres, cubes, and disks, for fcc packing. The Frenkel group (21, 22, 27) analyzed polyhedral fcc clusters of several different shapes and morphologies by using electron microscopy measurements of average size and EXAFS coordination numbers up to the fifth order. In this experiment, the authors constructed three-dimensional cluster models from which the coordination numbers were obtained through a suite of computer programs (27). Similarly, Roldan Cuenya et al. (28) compared EXAFS and electron microscopy data against a database of thousands of fcc clusters, including those with asymmetric shapes that can result from particle-substrate interactions. This method also enables higher-shell analysis. The common drawback of shape-specific calculation methods, however, is that the sequence of coordination numbers must be calculated for each individual cluster—a tedious process that does not take into account incomplete shells or disordered clusters.

Benfield (29), Fritsche & Benfield (30), and Montejano-Carrizales et al. (31) advanced this approach further by generating analytical equations for the coordination numbers as a function of cluster size for many geometries, including cuboctahedrons, icosahedrons, and tetrahedrons. The analytical equations yield accurate coordination-number values for these model shapes. However, the equations were derived for closed-shell clusters only and are shape specific, so they cannot be easily used to search for a specific size and shape if many geometries need to be compared. More importantly, these methods (with a few exceptions) were developed only for first-shell coordination-number analysis; the equations become very cumbersome for higher shells.

In addition to these exact approaches, several approximate methods have been developed. Jentys (32) simulated the coordination numbers with interpolated hyperbolic functions. The first five coordination numbers of computer-generated model nanoparticles of various sizes and shapes, including spheres, cubes, and distorted cubes, were modeled as a function of particle size with a hyperbolic function with four parameters calculated by fitting the obtained data points:

$$n_i = \frac{a N_{at}}{b + N_{at}} + \frac{c N_{at}}{d + N_{at}}, \tag{6}$$

where n_i is the coordination number for shell i; N_{at} is the number of atoms; and a, b, c, and d are the fitting parameters that can be obtained for each shape by fitting Equation 6 to the actual coordination numbers in a given family of clusters of the same shape but different N_{at}. For a few shapes (e.g., spheres, cubes, distorted cubes, and slabs, all with fcc packing), the graph of n_1 versus particle size did not differ greatly by shape; however, the graph of n_1/n_3 versus particle size is significantly shape dependent. According to Jentys, the particle size can be determined

RDF: radial distribution function

by comparing the first coordination number obtained from experimental EXAFS data with the fitted n_1 graph. The shape can be determined by comparing the n_1/n_3 versus particle size graph obtained from experimental EXAFS data with the fitted n_1/n_3 graph and determining whether the experimental curve falls above, on, or below the fitted curve. Unlike the exact methods, this approach uses a single equation to analyze all of the shapes studied, and because the equation was not derived for specific shapes, it does not need to assume complete shells. Additionally, coordination numbers up to the fifth shell can be determined. However, the obtained graphs, and the relationships between the coordination numbers that they contain, are limited to the three specific shapes; thus, general conclusions should be drawn with caution. Furthermore, other studies have demonstrated that some shapes do have a strong effect on first-shell coordination number, and thus such a method of size determination is limited to similar shapes (25). Jentys's coordination-number-ratio analysis was expanded by Beale & Weckhuysen (33), who included more shapes and employed a similar ratio analysis of different shell coordination numbers, thereby allowing for more specific shape determination.

Other methods estimate coordination numbers by assuming that nanoparticles are spherical. One such approach was developed by Calvin et al. (34), who derived an equation to determine coordination numbers as a function of cluster size:

$$n_{\text{nano}} = \left[1 - \frac{3}{4}\left(\frac{r}{R}\right) + \frac{1}{16}\left(\frac{r}{R}\right)^3\right] n_{\text{bulk}}, \tag{7}$$

where r is the distance between the nearest-neighbor atoms and R is the particle radius. This method allows one to calculate coordination numbers as a function of the cluster size for an arbitrary coordination shell (because r varies with the shell number), but it is limited to sufficiently large clusters. This method, in principle, can be used to discriminate between symmetric (quasi-spherical) and asymmetric clusters if the coordination numbers of the higher-order shells are measured by EXAFS.

Pirkkalainen & Serimaa (35) developed another approximate approach to determine coordination numbers up to the fourth shell for spherical nanoparticles of different sizes and different structures, including fcc, simple cubic, body-centered cubic, and hexagonal close-packed structures. The authors introduced an interpolation function, $y = 3t/r$, where t is the thickness of the surface-atom layer. The following equation was then used to determine the coordination number:

$$n_{\text{ave}} = (1 - y)n_{\infty} + y n_{\text{surf}}, \tag{8}$$

where n_{∞} is the theoretical coordination number for an infinite lattice and n_{surf} is the average contribution of surface atoms to the coordination number. The parameters t and n_{surf} are determined by fitting Equation 8 to the calculated coordination numbers. When compared with the exact methods, this approach provides accurate results, although the accuracy decreases for smaller particles because of the approximation for n_{surf} (**Figure 1**).

As mentioned above, all approximate methods can give reliable coordination-number values only if the nanoparticle is large and therefore can be considered spherical or, at least, symmetric. For small and/or asymmetric particles, the shape and the nature of the facets make a crucial difference in the coordination numbers, and more accurate methods of their calculations—those sensitive to the cluster shapes—are required.

Glasner & Frenkel (27) and Frenkel et al. (36) proposed an alternative approach to analytical methods that employed computer-generated clusters and the radial distribution function (RDF) procedure for calculating coordination numbers. The latter enables the rapid calculation of coordination numbers for an arbitrary coordination shell. For any model cluster, closed shell or not,

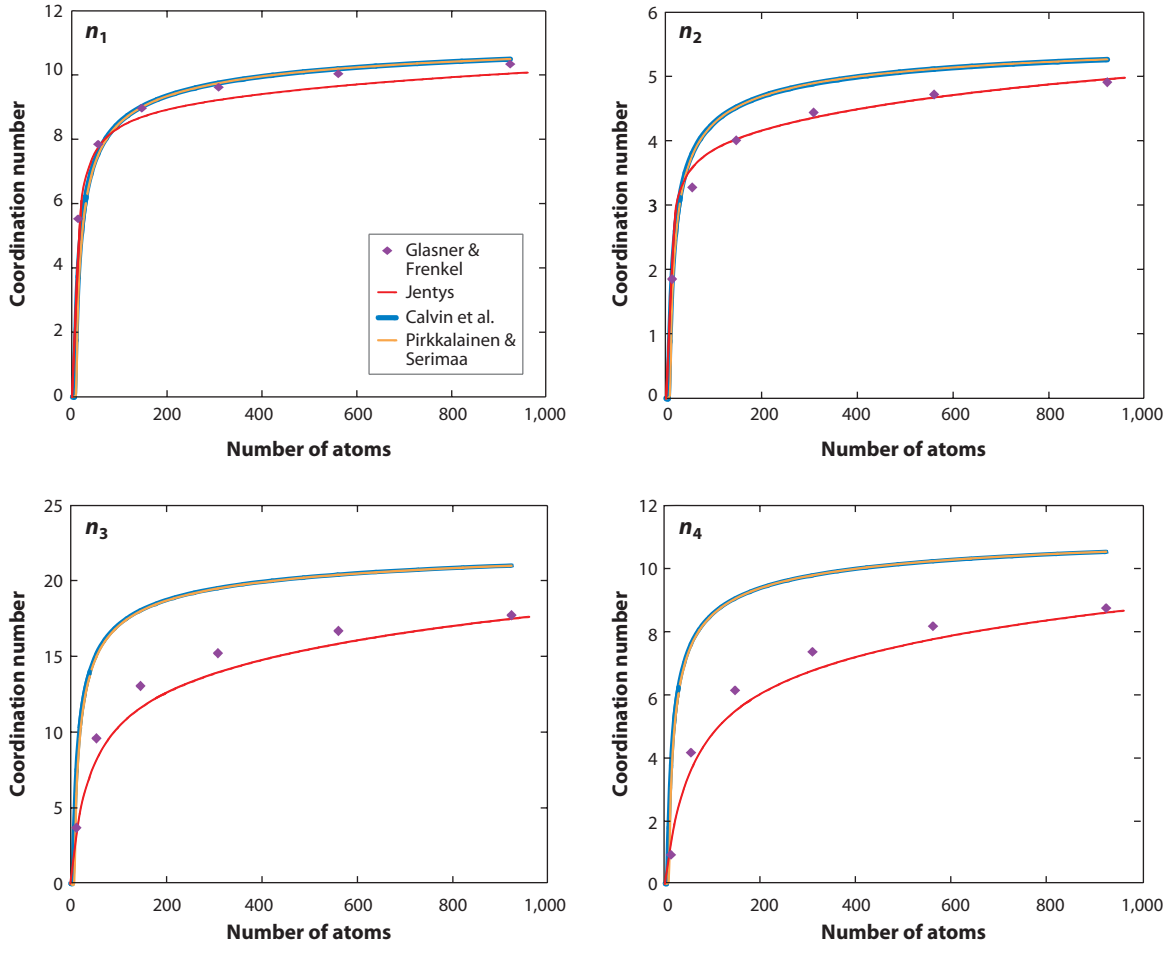

Figure 1

Coordination number of a face-centered cubic cuboctahedral particle versus particle size for various approximate approaches, compared with exact values (27). The approaches used by Calvin et al. (34) and Pirkkalainen & Serimaa (35) yield nearly identical approximations, as both assume spherical structures. Jentys's (32) approach most adequately reproduces coordination numbers in cuboctahedral clusters among all the approximate methods.

the frequency distribution of neighbors around a given atom is given by

$$\rho(r) = \frac{1}{N}\sum_{i=1}^{N}\rho_i(r), \tag{9}$$

with

$$\rho_i(r) = \frac{\Delta N_i}{\Delta R_i}, \tag{10}$$

where ρ_i is a partial RDF for an atom i and ΔN_i is the number of neighbors within the spherical shell of thickness ΔR_i. Integrating the RDF curve yields the average coordination numbers of the

absorbing atom for each shell over the entire sample

$$n_i = \int_{R_1}^{R_2} \rho(r) dr. \tag{11}$$

Equation 11 is equivalent to Equation 4 (and to Equation 5, for heterometallic pairs) but provides a fast, direct method of obtaining the coordination numbers of clusters with arbitrary sizes and shapes (including those with incomplete shells, as well as clusters in which the atomic positions are disordered). Many researchers combine electron microscopy data with multiple-scattering EXAFS analysis and data modeling to discriminate between several shapes with the same sequences (within the error bars) of the coordination numbers of the nearest-neighbor shells (25, 28, 32–34).

EXAFS also provides critical information about the structure of bimetallic nanoparticles. For a nanoparticle composed of atoms of types A and B, partial coordination numbers n_{AA}, n_{AB}, n_{BA}, and n_{BB} (defined above in Equations 4 and 5) can be measured by multiple-edge refinement of EXAFS data (37). These parameters elucidate the intraparticle composition, such as the extent of segregation or alloying of atoms (e.g., random distribution), as opposed to the positive or negative tendency to cluster (22, 23, 38–45). Once the above parameters are known, the total coordination number of metal-metal neighbors per absorbing atom can be determined from the following equation: $n_{MM} = x_A n_{AM} + x_B n_{BM}$ (23). The total coordination number can be employed to determine the size and shape by use of the same methods applied to monometallic particles. Alloys of elements with overlapping absorption edges (e.g., V and Cr, Pt and Ir, Pt and Au), however, cannot be analyzed simply by EXAFS because EXAFS at the higher-energy edge is convoluted with the EXAFS from the lower-energy edge. Menard et al. (46) recently proposed a simple solution in which the EXAFS from the two edges are deconvoluted with IFEFFIT.

Hwang et al. (47) developed a methodology to determine quantitatively the extent of alloying and dispersion in nanoparticles from EXAFS data. The authors' analysis uses the parameters $P_{observed}$, $R_{observed}$, P_{random}, and R_{random}, where $P_{observed}$ is defined as the ratio of n_{AB} to the total coordination number of metal neighbors to A atoms (n_{AM}). $R_{observed}$ is the ratio of n_{BA} to n_{BM}. P_{random} and R_{random} are the ratios for a perfectly alloyed particle, and both have a value of 0.5 if the ratio of the number of A atoms to B atoms is 1:1, which implies that $n_{AA} = n_{AB}$ and $n_{BB} = n_{BA}$. For different ratios of the number of A atoms to the number of B atoms, P_{random} and R_{random} can be easily determined (23). Parameter J_A is given by $J_A = \frac{P_{observed}}{P_{random}} \times 100\%$, and $J_B = \frac{R_{observed}}{R_{random}} \times 100\%$. By contrasting J_A and J_B with the coordination numbers n_{AA} and n_{BB}, one can resolve the details of the particle composition. For example, if $J_A < 100\%$ and $J_B < 100\%$ then A atoms "prefer" being adjacent to A atoms and B atoms "prefer" B atoms; that is, A and B atoms alloy less, indicating a positive tendency for clustering of like atoms. If $J_B > J_A$, then the core is A-rich, the shell is B-rich, and $n_{AA} > n_{BB}$; whereas if $J_A > J_B$, the core is B-rich, the shell is A-rich, and $n_{BB} > n_{AA}$.

For homogeneous alloys in which A and B atoms occur with equal probability within the particle or on the surface, $n_{AM} = n_{BM}$ (23). However, even in homogeneous alloys, short-range order may be present; it can be characterized by Cowley's short-range order parameter (48),

$$\alpha = 1 - \frac{N_{AB}/N_{AM}}{x_B}, \tag{12}$$

which was previously employed for EXAFS studies of bulk alloys (49). This parameter can be used to investigate the degree of the positive ($\alpha > 0$) or negative ($\alpha < 0$) tendency to clustering within the bimetallic nanoparticles (23).

The methods of Hwang et al. (47) and Frenkel (23) provide a general procedure for quantitatively analyzing atomic distributions. Importantly, the J_A and J_B criteria, as defined by Hwang et al., are meaningful only for sufficiently large clusters. We generalize this procedure to arbitrary cluster sizes in the next section.

4. STRUCTURAL AND COMPOSITIONAL DISORDER

The EXAFS data-modeling procedures summarized above yield accurate predictions for the geometric properties of nanoclusters if the following conditions are met:

1. All particles must be nearly identical in size and structure so that the ensemble-averaged environment of an absorbing atom is representative of that present in an individual nanoparticle.
2. The disorder in the interatomic distances must be quasi-Gaussian, ensuring that only a few leading cumulants (up to the third or fourth cumulant) are required to represent the unknown pair distribution function of neighbors. The bond-length disorder can be either intraparticle or interparticle in origin, or both.
3. For bimetallic particles, the interparticle compositional distribution must be sufficiently narrow so that the homogeneity and randomness of atomic species within the particles can be reliably characterized.

We address these conditions individually below.

4.1. Sample Heterogeneity

If the sample consists of a heterogeneous mixture of reduced and unreduced species, the best fit for the coordination numbers is related not only to the geometry of the particles but also to the volume fraction of the particles within the sample, which in such cases is less than 100% (23). In some cases, the size of the nanoparticles can be obtained independently by electron microscopy, and the analytical power of EXAFS is reduced to obtain merely the unknown volume fraction of the nanoparticles [from the ratio of the coordination numbers measured experimentally from EXAFS and calculated from the size obtained by electron microscopy, assuming a specific shape, such as round or polyhedral (50)].

4.2. Intraparticle Disorder

In most solids, the bond-length disorder is small to moderate throughout a wide temperature range. In nanoparticles, deviations from a perfect crystalline lattice are often enhanced relative to the bulk. Such deviations can result from capping ligands (51), steric effects (52), crystalline defects (e.g., twins) (53), multiple metastable states (54, 55), and interactions with adsorbates (56). The enhanced surface tension, typical in nanoparticles (57), causes a decrease in the lattice parameter (58–61). The most strained bonds are typically near the surface of the nanoparticle, which results in a strong variation (decrease) of the interatomic distances from the interior of the cluster toward the surface (59, 62). Such interparticle disorder is thus strongly non-Gaussian, which causes a problem in EXAFS analysis if such disorder is neglected in the model.

Yevick & Frenkel (63) recently accounted for anisotropic bond-length disorder through the following ansatz for the deviation of atomic positions, relative to the ideal periodic cluster, with the distance from the cluster center:

$$f(r) = A + (1 - A)\exp(Cr), \quad \text{where } C = \frac{1}{R}\ln\left(\frac{B - A}{1 - A}\right). \tag{13}$$

This distortion function satisfies the conditions $f(0) = 1$ and $f(R) = B \leq 1$ at the cluster center and the periphery, respectively. Multiplying all atomic coordinates by the distortion function (Equation 13) yields the new positions in the distorted cluster. The parameter A corresponds to the curvature of the distortion curve and can be changed, typically in the range between 1.05 and 1.00001, to simulate uniformly (59) and nonuniformly (62) distorted structures. The B parameter

typically lies in the range between 0.95 and 1.0, which agrees well with physically reasonable bond-length truncation effects in small clusters. The different distortion functions correspond to different distributions of the 1NN distances and simulate the radial relaxation of the surface tension from the outer layers of the cluster inward (**Figure 2*a***). Yevick & Frenkel (63) calculated the theoretical EXAFS signals in distorted and undistorted clusters and analyzed them by conventional methods that assume low disorder and include a third cumulant in the analysis. These authors concluded that

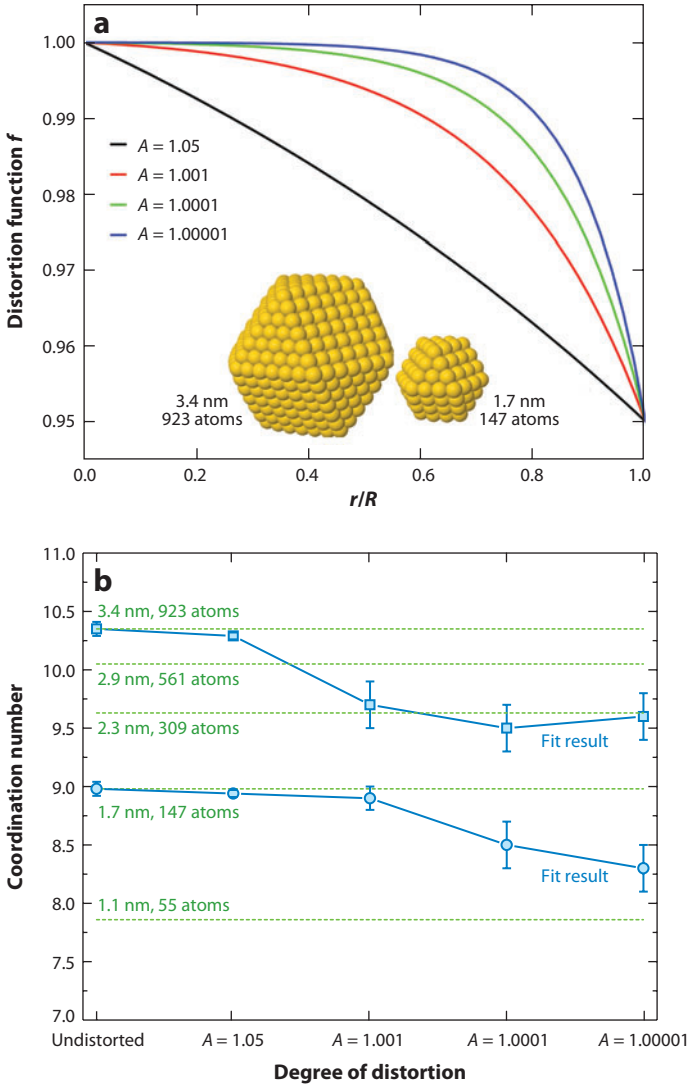

Figure 2

(*a*) Different distortion functions corresponding to $B = 0.95$. Two clusters of different sizes are shown; both are distorted with $A = 1.00001$ and $B = 0.95$. (*b*) Coordination numbers of the first-nearest neighbors obtained with quasi-Gaussian approximation by a FEFF6 fit to the data generated for model clusters of 147 and 923 atoms with different radial distortions A. Best-fit results are shown with symbols, and the model coordination numbers are shown as horizontal dashed lines. The solid lines are guides for the eye. Reproduced from Reference 63.

this non-Gaussian disorder may strongly bias EXAFS results. For example, the radial distortions similar to the one proposed by Huang et al. (62) cause the apparent coordination number to be 10% lower than the actual value if the distortions are not incorporated in the analysis (**Figure 2*b***).

The distortions and, thus, the errors resulting from neglecting the effects of surface relaxation can be minimized by passivating the particle surface with H_2 or CO, which increases bulk-like order in the clusters (13, 14, 64). To minimize errors in the coordination numbers and, hence, in the determined particle-size estimates (given that neglecting the disorder results in underestimation of the coordination numbers and, therefore, the size), complementary measurements obtained through other techniques are required.

4.3. Interparticle Disorder

The quantitative influence of the particle-size distribution on EXAFS measurements has not yet been studied, to the best of our knowledge. The general understanding is that EXAFS-derived coordination numbers overestimate the average cluster size if the size distribution is broad. If the distribution is known (e.g., from HAADF-STEM measurements), coordination numbers theoretically calculated for specific cluster models can be weighted with experimentally obtained cluster-size distribution to calculate the volume-weighted coordination numbers in nanoparticles. Such corrected coordination numbers can later be used for direct comparison with EXAFS results (64, 65).

We now consider a more general case of a symmetric arbitrary distribution of cluster order (L) that can be approximated as the Gaussian function

$$\rho(L) = \exp\left(-\frac{(L-\overline{L})^2}{2\sigma_s^2}\right), \tag{14}$$

where $\overline{L}$ is the average cluster order and σ_s is the standard deviation in L. In the calculations of coordination numbers below, we employ the cluster order [defined as the number of crusts in the cluster (31)] instead of the cluster size to insure that our results are independent of a given material composition. For cuboctahedral clusters, the cluster order L and cluster diameter D are simply related: $D = 2Lr$, where r is the 1NN distance. Because all the average quantities described below contain $\rho(L)$ both in the numerator and the denominator, the overall normalization constant of $\rho(L)$ is omitted from Equation 14. The subscript of σ designates the variance in the cluster order because a similar estimate of its influence on the coordination number measured by EXAFS is subsequently performed for the variance in the composition in heterometallic clusters (see below). We compare the theoretical coordination numbers in a cuboctahedral cluster of a certain order; the average coordination numbers are calculated over all clusters with the size distribution $\rho(L)$:

$$\tilde{n} = \frac{\int_0^\infty \rho(L)N(L)n(L)dL}{\int_0^\infty \rho(L)N(L)dL}. \tag{15}$$

Note that Equation 15 has a weighting factor, $N(L)$, which indicates the number of atoms in a cluster of the order L. This correction is required because $\rho(L)$ is commonly obtained by electron microscopy measurements as a frequency distribution that depends on cluster size, not volume, whereas volume averaging is required for coordination-number measurements by EXAFS.

To estimate the effect of $\rho(L)$ on the average coordination numbers, we assume cuboctahedral clusters in which the coordination number and the number of atoms for a given cluster order L are calculated as (31)

$$n(L) = \frac{24L(5L^2+3L+1)}{10L^3+15L^2+11L+3} \tag{16}$$

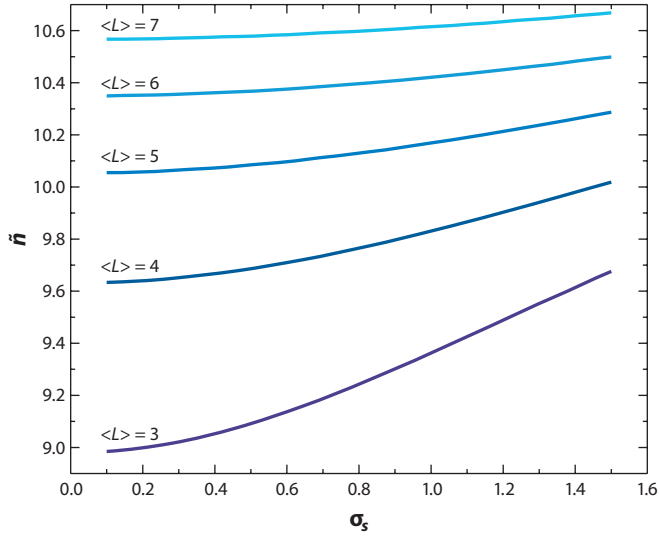

Figure 3

Apparent coordination number ($\tilde{n}$) as a function of the standard deviation of the size distribution (σ_s).

and

$$N(L) = \frac{10}{3}L^3 + 5L^2 + \frac{11}{3}L + 1. \quad (17)$$

Figure 3 shows the results obtained for $\tilde{n}$ as a function of σ_s, calculated for various values of $\overline{L}$. If $\sigma_s = 0$, then all clusters are identical and $\tilde{n} = n_0$, the coordination number in each cluster. For distributions $\rho(L)$ with nonzero σ_s, how are the EXAFS results different from those obtained for an equivalent cluster that has size $\overline{L}$ and coordination number n_0? When σ_s increases, $\tilde{n} > n_0$ because the larger clusters contribute more to the average than do the smaller clusters (Equation 15). As expected, for systems with relatively narrow size distributions—that is, with values of σ_s below 0.5 for small clusters and 1 for larger clusters—the EXAFS predictions are not significantly affected (**Figure 3**).

As a result, if the distribution of particle sizes is known, the average (theoretical) coordination numbers can be obtained by applying Equation 15. For quasi-Gaussian distributions, the average coordination numbers can be determined from **Figure 3** for different values of σ_s (here, we analyze several representative cluster orders). The experimenter measures σ_s, then determines both the intersection on the graph of σ_s and the measured coordination number to obtain an estimate of the mean cluster order and, thus, the mean cluster size. If σ_s is incorrectly assumed to be too narrow, the EXAFS coordination numbers overestimate the mean cluster size.

In summary, if the cluster-size distribution is broad, the above analysis must be performed to determine the coordination numbers in the equivalent (mean) cluster. Indeed, Equations 16 and 17 assume a specific shape of the cluster and therefore limit the generality of the coordination numbers that are obtained from Equation 15. However, EXAFS analysis is useful as a means to find out whether the microscopy and EXAFS results together point to the same model of the mean cluster in the distribution, with a certain size and shape. For example, suppose that a certain value for the coordination number is obtained by EXAFS and corrected through Equation 15, or **Figure 3**, to represent a mean cluster of the distribution. Then, assume that this value is very different from that inferred from the mean cluster size measured by electron microscopy. Such a

discrepancy must arise from other, unidentified factors. Thus, the EXAFS technique, even in this case, would yield important structural information.

Finally, there is the separate issue of the effects of σ_s on parameters such as the measured σ^2 (the Debye-Waller factor) or the measured r (the 1NN distance). These values are affected when larger clusters have different spacing between atoms, compared with the smaller clusters (66). We apply the same formula as Equation 15 but replace $n(L)$ with $r(L)$, which is the average spacing between atoms for a given cluster order. This quantity is system dependent and difficult to obtain because it should be measured in a series of well-defined clusters of different average sizes. We have observed that, even for very poorly defined cluster sizes, with $\sigma_s/L \approx 2/3$ and typical choices of $r(L)$, the resulting corrections do not exceed 0.015 Å for r and 0.00015 Å^2 for σ^2. These effects therefore require less attention compared with other factors that affect EXAFS results.

4.4. Compositional Disorder in Bimetallic Nanoparticles

We demonstrated in the previous section that knowledge of partial coordination numbers in heterometallic nanoparticles provides detailed insight into the nanoparticles' compositional habits; this information includes the degree of the short-range order and the homogeneity of alloying. In this section, we quantify the effects of compositional disorder on the EXAFS analysis results and demonstrate that interparticle variations in the composition affect the experimentally determined coordination numbers.

For simplicity, we consider a system that contains particles of the same size but in which the particle composition varies around the average value from cluster to cluster. We take the distribution of composition to be a Gaussian in x:

$$\rho(x) = \exp\left(-\frac{(x-\bar{x})^2}{2\sigma_c^2}\right), \tag{18}$$

where $x = N_A/N$ is the fraction of atoms that are of type A in a given cluster, $\bar{x}$ is the average composition over all clusters, and σ_c represents the standard deviation in the distribution of $\rho(x)$. Furthermore, we assume a random ordering of the atoms within each cluster.

Because of the random distribution of atoms, the partial coordination number n_{AA} in each cluster is defined as

$$n_{AA} = \frac{N_A - 1}{N - 1} n_{MM}, \tag{19}$$

where N_A is the number of atoms of type A in the given cluster, and N is the total number of atoms in each cluster (which is identical for all clusters as a result of the identical cluster sizes). Equation 19 is more general than the equations used by Hwang et al. (47) and Frenkel (23), which require that $n_{AA} = x n_{MM}$ for randomly distributed atoms within the clusters. The previous approaches agree with Equation 19 for clusters with a large number of atoms, but only for values of x that are not too close to the boundaries of the compositional range (zero and one), whereas Equation 19 is accurate for all clusters and also correctly calculates the coordination numbers over the entire compositional range. The exact formulas for the partial coordination numbers, averaged over the ensemble of clusters, are

$$\tilde{n}_{AA} = \frac{\int_0^1 \rho(x) x n_{AA}(x) dx}{\int_0^1 \rho(x) x dx} \tag{20}$$

and

$$\tilde{n}_{AB} = n_{MM} - \tilde{n}_{AA} = n_{AM} - \tilde{n}_{AA}. \tag{21}$$

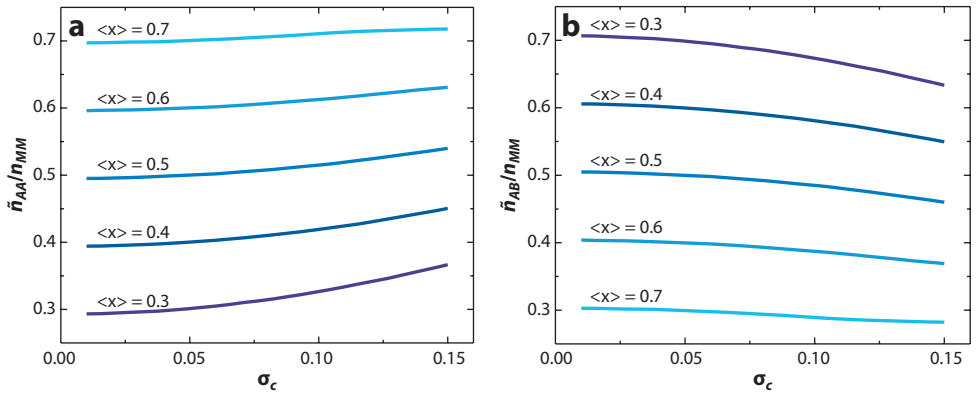

Figure 4

Normalized partial coordination numbers of (*a*) *AA* and (*b*) *AB* pairs as functions of the standard deviation of the cluster composition for clusters of $N = 100$ atoms, calculated assuming a Gaussian compositional distribution.

Calculated partial coordination numbers (for clusters with $N = 100$ atoms, where we have normalized the resultant coordination numbers by n_{MM}) are shown in **Figure 4**. Our results indicate that the ensemble-average coordination numbers $\tilde{n}_{AA}$ can be smaller for narrow compositional distributions or larger for broad distributions than the coordination numbers predicted by the equation $n_{AA} = xn_{MM}$. The two sets of values, $\tilde{n}_{AA}$ and n_{AA}, agree for $\sigma_c = \sqrt{x(1-x)/N}$, for which the normal distribution coincides with binomial distribution.

SUMMARY POINTS

1. Comparing the coordination numbers obtained from multiple-scattering EXAFS analysis for a few nearest-neighboring shells against a large number of available polyhedral cluster models, then determining the structure that best matches the EXAFS results, yields in principle the three-dimensional structure, shape, and compositional distribution of a cluster.
2. The structural refinement of EXAFS data is complicated by disorder in the atomic positions. These effects can be corrected for small and/or Gaussian disorder. In many nanoparticle systems, however, the disorder is asymmetric as a result of surface reconstruction or interior defects such as dislocations or twins, so additional analysis is required to extract accurate coordination numbers.
3. To identify the structure and shape of the equivalent (mean) cluster, the broad size distribution of nanoparticles in a sample requires further corrections to the EXAFS coordination numbers.
4. Partial coordination numbers in a heterometallic particle can be employed to quantify the intraparticle homogeneity and short-range order for arbitrary cluster sizes and a wide range of component fractions, provided that all the clusters possess nearly identical compositions.
5. If the composition varies widely from cluster to cluster, corrections can be applied to characterize the equivalent (mean) cluster of the sample.

DISCLOSURE STATEMENT

The authors are not aware of any affiliations, memberships, funding, or financial holdings that might be perceived as affecting the objectivity of this review.

ACKNOWLEDGMENTS

The authors acknowledge financial support from the Office of Basic Energy Sciences of the U.S. Department of Energy under grant number DE-FG02-03ER15476. A.Y. and C.C. greatly appreciate travel support from the Department of Energy's Synchrotron Catalysis Consortium (grant number DE-FG02-05ER15688). A.Y. gratefully acknowledges support from the Dr. Henry Kressel Scholarship at Yeshiva University. C.C. was supported in part by the Catalysis Center for Energy Innovation, an Energy Frontier Research Center funded by the U.S. Department of Energy, Office of Science, Office of Basic Energy Sciences, under award number DE-SC00010004.

LITERATURE CITED

1. Sayers DE, Stern EA, Lytle FW. 1971. New technique for investigating noncrystalline structures: Fourier analysis of the extended X-ray absorption fine structure. *Phys. Rev. Lett.* 27:1204–7
2. Lytle FW, Via GH, Sinfelt J. 1977. Determination of structure of Cu and Cu-Ru on carriers using X-ray absorption spectroscopy. *Erdöl Kohle Erdgas Petrochem.* 30:231
3. Sinfelt JH, Via GH, Lytle FW. 1978. Extended X-ray absorption fine-structure (EXAFS) of supported platinum catalysts. *J. Chem. Phys.* 68:2009–10
4. Meitzner G, Via GH, Lytle FW, Sinfelt JH. 1983. Structure of bimetallic clusters—extended X-ray absorption fine-structure (EXAFS) studies of Rh-Cu clusters. *J. Chem. Phys.* 78:882–89
5. Meitzner G, Via GH, Lytle FW, Sinfelt JH. 1987. Structure of bimetallic clusters—extended X-ray absorption fine-structure (EXAFS) of Pt-Re and Pd-Re clusters. *J. Chem. Phys.* 87:6354–63
6. Treacy MMJ, Rice SB. 1989. Catalyst particle sizes from Rutherford scattered intensities. *J. Microsc.* 156:211–34
7. Singhal A, Yang JC, Gibson JM. 1997. STEM-based mass spectroscopy of supported Re clusters. *Ultramicroscopy* 67:191–206
8. Zabinsky SI, Rehr JJ, Ankudinov A, Albers RC, Eller MJ. 1995. Multiple-scattering calculations of X-ray absorption spectra. *Phys. Rev. B* 52:2995–3009
9. Bunker G. 1983. Application of the ratio method of EXAFS analysis to disordered systems. *Nucl. Instrum. Methods* 207:437–44
10. Rehr JJ, Albers RC. 2000. Theoretical approaches to X-ray absorption fine structure. *Rev. Mod. Phys.* 72:621–54
11. Crozier ED, Rehr JJ, Ingalls R. 1988. Amorphous and liquid systems. In *X-Ray Absorption Spectroscopy*, ed. DC Koningsberger, R Prins, pp. 373–442. New York: Wiley
12. Bus E, Miller JT, Kropf AJ, Prins R, van Bokhoven JA. 2006. Analysis of in situ EXAFS data of supported metal catalysts using the third and fourth cumulant. *Phys. Chem. Chem. Phys.* 8:3248–58
13. Kang JH, Menard LD, Nuzzo RG, Frenkel AI. 2006. Unusual non-bulk properties in nanoscale materials: thermal metal-metal bond contraction of γ-alumina-supported Pt catalysts. *J. Am. Chem. Soc.* 128:12068–69
14. Sanchez SI, Menard LD, Bram A, Kang JH, Small MW, et al. 2009. The emergence of nonbulk properties in supported metal clusters: negative thermal expansion and atomic disorder in Pt nanoclusters supported on γ-Al_2O_3. *J. Am. Chem. Soc.* 131:7040–54
15. Frenkel AI, Rehr JJ. 1993. Thermal expansion and X-ray absorption fine-structure cumulants. *Phys. Rev. B* 48:585–88
16. Sevillano E, Meuth H, Rehr JJ. 1979. Extended X-ray absorption fine-structure Debye-Waller factors. I. Monatomic crystals. *Phys. Rev. B* 20:4908–11
17. Brillouin L. 1962. *Science and Information Theory*. New York: Academic

18. Ravel B, Newville M. 2005. ATHENA, ARTEMIS, HEPHAESTUS: data analysis for X-ray absorption spectroscopy using IFEFFIT. *J. Synchrotron Radiat.* 12:537–41
19. Gurman SJ, Binsted N, Ross I. 1984. A rapid, exact curved-wave theory for EXAFS calculations. *J. Phys. C* 17:143–51
20. Filipponi A, Di Cicco A, Natoli CR. 1995. X-ray-absorption spectroscopy and *n*-body distribution functions in condensed matter. I. Theory. *Phys. Rev. B* 52:15122–34
21. Frenkel AI. 1999. Solving the structure of nanoparticles by multiple-scattering EXAFS analysis. *J. Synchrotron Radiat.* 6:293–95
22. Nashner MS, Frenkel AI, Adler DL, Shapley JR, Nuzzo RG. 1997. Structural characterization of carbon-supported platinum-ruthenium nanoparticles from the molecular cluster precursor $PtRu_5C(CO)_{16}$. *J. Am. Chem. Soc.* 119:7760–71
23. Frenkel A. 2007. Solving the 3D structure of metal nanoparticles. *Z. Kristallogr.* 222:605–11
24. Via GH, Drake KF, Meitzner G, Lytle FW, Sinfelt JH. 1990. Analysis of EXAFS data on bimetallic clusters. *Catal. Lett.* 5:25–33
25. Frenkel AI, Hills CW, Nuzzo RG. 2001. A view from the inside: complexity in the atomic scale ordering of supported metal nanoparticles. *J. Phys. Chem. B* 105:12689–703
26. Greegor RB, Lytle FW. 1980. Morphology of supported metal clusters—determination by EXAFS and chemisorption. *J. Catal.* 63:476–86
27. Glasner D, Frenkel AI. 2007. Geometrical characteristics of regular polyhedra: application to EXAFS studies of nanoclusters. *Am. Inst. Phys. Conf. Proc.* 882:746–48
28. Roldan Cuenya B, Croy JR, Mostafa S, Behafarid F, Li L, et al. 2010. Solving the structure of size-selected Pt nanocatalysts synthesized by inverse micelle encapsulation. *J. Am. Chem. Soc.* 132:8747–56
29. Benfield RE. 1992. Mean coordination numbers and the nonmetal metal transition in clusters. *J. Chem. Soc. Faraday Trans.* 88:1107–10
30. Fritsche HG, Benfield RE. 1993. Exact analytical formulas for mean coordination numbers in clusters. *Z. Phys. D* 26:S15–S17
31. Montejano-Carrizales JM, Aguilera-Granja F, Moran-Lopez JL. 1997. Direct enumeration of the geometrical characteristics of clusters. *Nanostruct. Mater.* 8:269–87
32. Jentys A. 1999. Estimation of mean size and shape of small metal particles by EXAFS. *Phys. Chem. Chem. Phys.* 1:4059–63
33. Beale AM, Weckhuysen BM. 2010. EXAFS as a tool to interrogate the size and shape of mono and bimetallic catalyst nanoparticles. *Phys. Chem. Chem. Phys.* 12:5562–74
34. Calvin S, Miller MM, Goswami R, Cheng SF, Mulvaney SP, et al. 2003. Determination of crystallite size in a magnetic nanocomposite using extended X-ray absorption fine structure. *J. Appl. Phys.* 94:778–83
35. Pirkkalainen K, Serimaa R. 2009. Coordination number in ideal spherical nanocrystals. *J. Appl. Crystallogr.* 42:442–47
36. Frenkel AI, Frankel SC, Liu TB. 2005. Structural stability of giant polyoxomolybdate molecules as probed by EXAFS. *Phys. Scr.* T115:721–23
37. Frenkel AI, Stern EA, Voronel A, Heald SM. 1996. Lattice strains in disordered mixed salts. *Solid State Commun.* 99:67–71
38. Nashner MS, Frenkel AI, Somerville D, Hills CW, Shapley JR, Nuzzo RG. 1998. Core shell inversion during nucleation and growth of bimetallic Pt/Ru nanoparticles. *J. Am. Chem. Soc.* 120:8093–101
39. Hills CW, Nashner MS, Frenkel AI, Shapley JR, Nuzzo RG. 1999. Carbon support effects on bimetallic Pt-Ru nanoparticles formed from molecular precursors. *Langmuir* 15:690–700
40. Knecht MR, Weir MG, Frenkel AI, Crooks RM. 2008. Structural rearrangement of bimetallic alloy PdAu nanoparticles within dendrimer templates to yield core/shell configurations. *Chem. Mater.* 20:1019–28
41. Weir MG, Knecht MR, Frenkel AI, Crooks RM. 2010. Structural analysis of PdAu dendrimer–encapsulated bimetallic nanoparticles. *Langmuir* 26:1137–46
42. Toshima N, Harada M, Yonezawa T, Kushihashi K, Asakura K. 1991. Structural analysis of polymer-protected Pd/Pt bimetallic clusters as dispersed catalysts by using extended X-ray absorption fine-structure spectroscopy. *J. Phys. Chem.* 95:7448–53
43. Toshima N, Yonezawa T. 1998. Bimetallic nanoparticles—novel materials for chemical and physical applications. *New J. Chem.* 22:1179–201

44. Harada M, Asakura K, Toshima N. 1994. Structural-analysis of polymer-protected platinum/rhodium bimetallic clusters using extended X-ray absorption fine-structure spectroscopy—importance of microclusters for the formation of bimetallic clusters. *J. Phys. Chem.* 98:2653–62
45. Asakura K, Bian CR, Suzuki S, Chun WJ, Watari N, et al. 2005. An XAFS study on the polymer protected CuPd bimetallic nanoparticles—a novel heterobond-philic structure. *Phys. Scr.* T115:781–83
46. Menard LD, Wang Q, Kang JH, Sealey AJ, Girolami GS, et al. 2009. Structural characterization of bimetallic nanomaterials with overlapping X-ray absorption edges. *Phys. Rev. B* 80:064111
47. Hwang BJ, Sarma LS, Chen JM, Chen CH, Shih SC, et al. 2005. Structural models and atomic distribution of bimetallic nanoparticles as investigated by X-ray absorption spectroscopy. *J. Am. Chem. Soc.* 127:11140–45
48. Cowley JM. 1965. Short-range order and long-range order parameters. *Phys. Rev.* 138:A1384–89
49. Frenkel AI, Machavariani VS, Rubshtein A, Rosenberg Y, Voronel A, Stern EA. 2000. Local structure of disordered Au-Cu and Au-Ag alloys. *Phys. Rev. B* 62:9364–71
50. Sun Y, Frenkel AI, Isseroff R, Shonbrun C, Forman M, et al. 2006. Characterization of palladium nanoparticles by using X-ray reflectivity, EXAFS, and electron microscopy. *Langmuir* 22:807–16
51. Carter AC, Bouldin CE, Kemner KM, Bell MI, Woicik JC, Majetich SA. 1997. Surface structure of cadmium selenide nanocrystallites. *Phys. Rev. B* 55:13822–28
52. Shiang JJ, Kadavanich AV, Grubbs RK, Alivisatos AP. 1995. Symmetry of annealed wurtzite CdSe nanocrystals—assignment to the C3v point group. *J. Phys. Chem.* 99:17417–22
53. Diaz de la Rubia T, Gilmer G. 2002. Cluster nucleation: watching nanoclusters nucleate. *Nat. Mater.* 1:89–90
54. Wang L-L, Johnson DD. 2007. Density functional study of structural trends for late-transition-metal 13-atom clusters. *Phys. Rev. B* 75:235405–14
55. Chernyshev A. 2008. Melting of surface layers of nanoparticles: Landau model. *Mater. Chem. Phys.* 112:226–29
56. Lopez-Cartes C, Rojas TC, Litran R, Martinez-Martinez D, de la Fuente JM, et al. 2005. Gold nanoparticles with different capping systems: an electronic and structural XAS analysis. *J. Phys. Chem. B* 109:8761–66
57. Mays CW, Vermaak JS, Kuhlmann D. 1968. On surface stress and surface tension. II. Determination of surface stress of gold. *Surf. Sci.* 12:134–40
58. Purdum H, Montano PA, Shenoy GK, Morrison T. 1982. Extended X-ray absorption fine-structure study of small Fe molecules isolated in solid neon. *Phys. Rev. B* 25:4412–17
59. Woltersdorf J, Nepijko AS, Pippel E. 1981. Dependence of lattice parameters of small particles on the size of the nuclei. *Surf. Sci.* 106:64–69
60. Qi WH, Wang MP, Su YC. 2002. Size effect on the lattice parameters of nanoparticles. *J. Mater. Sci. Lett.* 21:877–78
61. Lamber R, Wetjen S, Jaeger NI. 1995. Size dependence of the lattice parameter of small palladium particles. *Phys. Rev. B* 51:10968–71
62. Huang WJ, Sun R, Tao J, Menard LD, Nuzzo RG, Zuo JM. 2008. Coordination-dependent surface atomic contraction in nanocrystals revealed by coherent diffraction. *Nat. Mater.* 7:308–13
63. Yevick A, Frenkel AI. 2010. Effects of surface disorder on EXAFS modeling of metallic clusters. *Phys. Rev. B* 81:11451–57
64. Guo N, Fingland BR, Williams WD, Kispersky VF, Jelic J, et al. 2010. Determination of CO, H_2O and H_2 coverage by XANES and EXAFS on Pt and Au during water gas shift reaction. *Phys. Chem. Chem. Phys.* 12:5678–93
65. Menard LD, Xu HP, Gao SP, Twesten RD, Harper AS, et al. 2006. Metal core bonding motifs of monodisperse icosahedral Au_{13} and larger Au monolayer–protected clusters as revealed by X-ray absorption spectroscopy and transmission electron microscopy. *J. Phys. Chem. B* 110:14564–73
66. Frenkel AI, Nemzer S, Pister I, Soussan L, Harris T, et al. 2005. Size-controlled synthesis and characterization of thiol-stabilized gold nanoparticles. *J. Chem. Phys.* 123:184701–6

Annual Review of
Analytical Chemistry

Volume 4, 2011

Contents

Indexes

Errata

An online log of corrections to the *Annual Review of Analytical Chemistry* articles may be found at http://arjournals.annualreviews.org/errata/anchem